



## Physical structure of the Barents Sea Polar Front near Storbanken in August 2007

S. Våge<sup>a,b,\*</sup>, S.L. Basedow<sup>b,c</sup>, K.S. Tande<sup>c</sup>, M. Zhou<sup>d</sup>

<sup>a</sup> Department of Biology, University of Bergen, Norway

<sup>b</sup> Faculty of Biosciences, Fisheries and Economics, University of Tromsø, Norway

<sup>c</sup> Faculty of Biosciences and Aquaculture, University of Nordland, Norway

<sup>d</sup> Department of Environmental, Earth and Ocean Sciences, University of Massachusetts Boston, USA

### ARTICLE INFO

#### Article history:

Received 8 February 2011

Received in revised form 21 November 2011

Accepted 24 November 2011

Available online 2 December 2011

#### Keywords:

Barents Sea Polar Front

Storbanken

Hydrography

Currents

High-resolution survey

Sub-mesoscale variability

### ABSTRACT

The Polar Front separating Atlantic Water (AW) and Arctic Water (ArW) is one of the most dominant meso- and large scale features in the Barents Sea. Here, the results of submeso-mesoscale (1–10 km) variability in physical fields associated with the Barents Sea Polar Front (BSPF) are reported from a high-resolution ADCP (Acoustic Doppler Current Profiler) and CTD (Conductivity–Temperature–Depth sensors) survey near Storbanken in August 2007. A surface front separating AW and melt water with a strong salinity gradient was present, while the subsurface BSPF was characterized by a strong temperature gradient and thermohaline compensation. Isopycnal mixing leading to the formation of Polar Front Water (PFW) was observed. The dominant flow was a barotropic southeastward along-frontal jet with two cores, coinciding with the surface front and the BSPF. This gives new insights into the circulation at the BSPF. Small-scale variability in the hydrographic and dynamic structures was observed, which were rarely resolved in previous cruises. Such submeso-mesoscale physical processes can potentially have significant impacts on the biogeochemistry and biology in the area, indicating the importance of parametrizing the processes in future climate models.

© 2011 Elsevier B.V. All rights reserved.

### 1. Introduction

Fronts have become areas of great interest to the oceanographic community, as frontal processes are now understood to be important for both global climate through thermohaline and gyre circulation in the open ocean, and regional processes such as upwelling and demarcation of marine ecosystems (Belkin et al., 2009; Rixen et al., 2003). High-resolution measurements are necessary to resolve submeso-mesoscale (1–10 km) processes and dynamics associated with fronts. A large scale ocean-atmosphere climate model without adequate parameterization of submeso-mesoscale processes may underestimate the poleward heat transport and the ecosystem productivity (Fanning and Weaver, 1997; Hansen and Samuelsen, 2009).

In the Nordic seas, the North Polar Frontal Zone (NPFZ) is a major climatic feature (Rodionov, 1992). It is located at the interface between the northward extension of the comparatively warm and saline Atlantic Water (AW) and the southward extension of the cool and relatively fresh Arctic Water (ArW). One branch of the AW enters into the Barents Sea via the North Cape Current along the northern coast of Norway before leaving through the Bear Island Trough (Gawarkiewicz and Plueddemann, 1995). The ArW flows into the Barents Sea between Spitsbergen and Franz Josef Land via the East

Spitsbergen Current and between Franz Josef Land and Novaya Zemlya via the Persey Current before exiting westward through the Bear Island Current (Loeng, 1991). Variations in transports and properties of the AW and ArW inflows strongly influence the hydrographic and climatic properties of the Barents Sea (Furevik, 2001; Ingvaldsen et al., 2002; Sakshaug, 1997).

The Barents Sea Polar Front (BSPF), which occurs at the boundary between the Atlantic and the Arctic currents, is part of the NPFZ and the dominant meso- and large-scale feature of the Barents Sea. It is the southern border for sea ice and an area of formation of Polar Front Water (PFW) through mixing between the AW and the ArW (Harris et al., 1998; Loeng, 1991). Topographic steering determines the position of the front. Particularly in the west, the BSPF closely follows the southern flank of Spitsbergenbanken near the 260-m isobath (Gawarkiewicz and Plueddemann, 1995). The BSPF extends along the northwestern side of the Bear Island Trough and the Hopen Trench towards Storbanken, where it turns south to follow the eastern flank of Sentralbanken before turning east, covering a total distance of approximately 1500 km (Johannessen and Foster, 1978) (Fig. 1, top). In the eastern Barents Sea, the front is a broader zone of mixing (Harris et al., 1998; Ingvaldsen, 2005).

The general location of the BSPF was first determined based on temperature gradient criteria in summer 1974 (Johannessen and Foster, 1978). Hydrographic and flow properties of the BSPF were investigated with 10 km resolution during the Barents Sea Polar Front Experiment (BSPFE) at the southern flank of Spitsbergenbanken in summer 1992 (Gawarkiewicz and Plueddemann, 1995; Parsons et

\* Corresponding author at: Department of Biology, University of Bergen, Norway. Tel.: +47 942 135 81.

E-mail addresses: [selina.vage@bio.uib.no](mailto:selina.vage@bio.uib.no) (S. Våge), [sunnje.basedow@uin.no](mailto:sunnje.basedow@uin.no) (S.L. Basedow), [kurt.tande@uin.edu](mailto:kurt.tande@uin.edu) (K.S. Tande), [meng.zhou@umb.edu](mailto:meng.zhou@umb.edu) (M. Zhou).

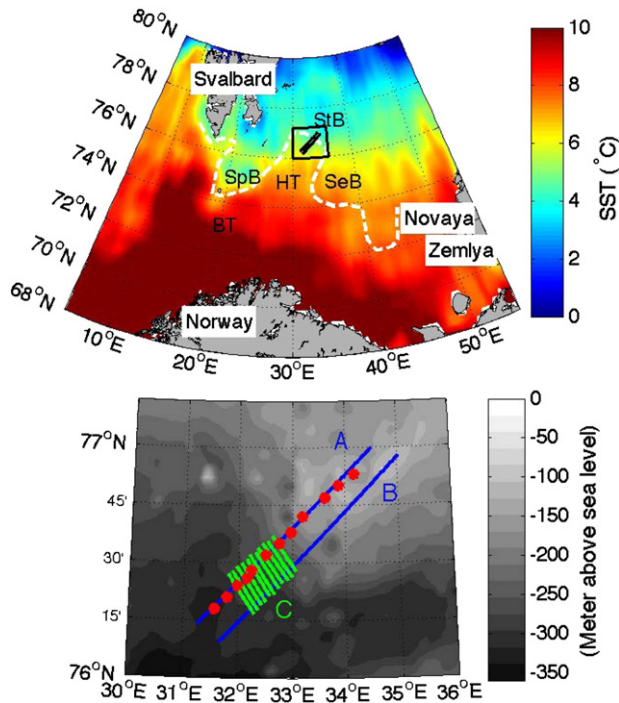


**Fig. 1.** Top: Sea surface temperature (SST) in the Barents Sea on August 15, 2007 (data from the National Climate Data Center, <http://www.ncdc.noaa.gov/oa/climate/research/sst/oi-daily.php>). The mean frontal position of the Polar Front is shown as a white dashed line (based on Loeng, 1991). BT = Bear Island Trough, SpB = Spitsbergenbanken, HT = Hopen Trench, StB = Storbanken, SeB = Sentralbanken. Sampling sections near Storbanken are shown in the black box (blown up at the bottom). Bottom: Bathymetry (ETOPO2 data set, <http://sos.noaa.gov/datasets/Land/etopo2.html>) in the study area with cross-frontal sampling sections A and B, along-frontal sampling sections C, and full-depth CTD stations (red dots).

al., 1996). A shallower mixed layer was observed on the northern (Arctic) side of the front, where the stratification was stronger due to ice melt, and a horizontal density gradient near the surface was established due to the cross-frontal salinity gradient. At depth, the cross-frontal temperature gradient was pronounced and thermohaline compensation eliminated the density gradient, resulting in a nearly barotropic front (Parsons et al., 1996). The thermohaline structure observed during the BSPFE was generally consistent with previous surveys of the BSPF (Berezutskii et al., 1994; Johannessen and Foster, 1978).

While previous studies also agree on the southwestward flow of the ArW in the Bear Island current north of the BSPF, the AW flow south of the front is more controversial. Some observational and modeling studies suggest an eastward warm-core jet of AW on the southeastern flank of Spitsbergenbanken near the 300-m isobath, and a southward flow of AW and ArW along the Polar Front southeast of Sentralbanken (Li and McClimans, 1998; Loeng, 1991; McClimans and Nilsen, 1993). This eastward flow direction is in good agreement with earlier observations (Johansen et al., 1988; Loeng et al., 1989). Geostrophic calculations from the BSPFE, on the other hand, indicate only a weak eastward geostrophic flow on the Atlantic side of the front, between the 150 and 200 m isobaths (Parsons et al., 1996). Between the 260 and 400 m isobaths, a westward flow of AW was observed, in contrast to the results by Li and McClimans (1998). This westward flow was reproduced by a modeling study and attributed to recirculating AW within the Bear Island Trough (Gawarkiewicz and Plueddemann, 1995). Li and McClimans consider the westward flow of the AW observed in the BSPFE to be a result of seasonal sea level differences induced by seasonal wind fields or variation of freshwater discharge from Russia, while they suggest a predominately eastward flow direction of the AW along the flank of Spitsbergenbanken.

Using the high-resolution data from our survey in the frontal area at Storbanken, this contentious issue about the flow direction of the AW south of the BSPF is studied. The purpose of this study is to provide a detailed description of the hydrographic and dynamic structure of the BSPF at the southwestern flank of Storbanken. Based on a high-resolution three-dimensional data set, novel insights into the submesoscale variability in the physical fields associated with the front will be given.

## 2. Data and methods

### 2.1. Field sampling

Data were collected in the Barents Sea from RV “Jan Mayen” in the frontal area near Storbanken (~76–77°N and 31–35°E) from August 8 to August 15, 2007 (Fig. 1, bottom). The area of the Polar Front was sampled along two cross-frontal sections (sections A and B, 119 and 125 km long, respectively) and 12 along-frontal sections (C sections, 20–23 km long each). The cross- and along-front sections were surveyed using a ship-mounted 76.8 kHz Broad Band Ocean Surveyor Acoustic Doppler Current Profiler (ADCP, Teledyne RD Instruments, CA, USA) and an undulating, towed instrument platform (Scanfish, MacArtney Inc., Esbjerg, Denmark) equipped with SBE911 plus Conductivity–Temperature–Depth sensors (CTD, Sea-Bird Electronics, WA, USA).

The ship-mounted ADCP continuously recorded data at a rate of one ping per second while the ship was moving at about 7 knots. The bin length was set to 16 m and the transducer depth was 7 m below the surface. Twenty bins were measured in the vertical, giving the ADCP a nominal range between 23 m and 327 m, while the bottom was never deeper than 305 m. Simultaneously to the ADCP recordings, the Scanfish platform undulated between 2 and 3 m below the surface and 75 m (referred to Scanfish layer below), logging hydrographic data at 2 Hz. This depth range was chosen to include the mixed layer (which was shallower than 30 m), to fully cover the surface front, and to maximize the horizontal resolution at the front.

The two cross-frontal sections A and B were sampled within 20 h between August 8 and August 9, 2007. Data from the C sections represent a synoptic survey, although true synopticity could not be achieved as the survey period was about 24 h between August 13 and August 14. The area covered by the C sections was roughly 20 × 30 km and had a horizontal resolution of 2.7 km and higher (the horizontal spacing between undulations was about 1 km).

Twelve full-depth CTD stations along section A were sampled with a spacing between 5 and 10 km in addition to the ADCP and Scanfish sections. They were conducted between August 14 and August 15 using a Sea-Bird SBE911 plus CTD profiler. CTD data were processed to a vertical interval of 1 decibar (db) using the standard Sea-Bird procedures. For each station, one water sample was taken from the deepest bottle of a 12 position SBE32 rosette with 5 l sampling bottles to calibrate the salinity sensor.

### 2.2. Data processing

Due to a malfunctioning of the link between the ship heading and the ADCP instrument, eastward and northward velocity components in the absolute earth coordinate system were not produced during data recording. This forced us to use the ship-coordinate system for the velocity components instead (the two reciprocal pairs of transducer beams were configured to point in the along- and cross-track direction, respectively). Since information on the heading, pitch and roll angles were missing, the velocity components in the ship coordinate system could not be corrected for the multi-scale variations in the ship orientation. For this analysis, we assume a straight line ship's heading based on the start and end locations for each section.

The ADCP velocity components in the along-track direction contained a significant amount of noise and were omitted entirely from the data analysis. The data in the cross-track direction were corrected from the cross-track ship speed component using bottom track velocities. A five-minute ensemble average was applied for improving measurement accuracies. Based upon the manufacturer's accuracy estimate, the data have a velocity accuracy (95% confidence interval) of about  $0.02\text{--}0.03\text{ m s}^{-1}$ . All data from the first bin and from the zone above the bottom, which made up 15% of the distance between the transducer and the bottom, were discarded. They are known to have a low signal-to-noise ratio due to ringing effects and erroneous bottom signals, respectively. Finally, data outside the range of  $\pm 2$  standard deviations from the mean velocity in each 5 min ensemble were excluded.

The influence of tides was studied using the Arctic Ocean Tidal Inverse Model that has a horizontal resolution of 5 km (AOTIM5) (Padman and Erofeeva, 2004). Cross-track tidal velocity components were obtained from the model by rotating the reference frame from the earth coordinates to the along- and cross-section coordinates. For each section, a straight line was fitted through all ensemble positions. From this line, the starting and end positions of the straight section were determined and the rotation angle  $\gamma$  was computed. The cross-track tidal velocity components were subtracted from the measured cross-track ADCP components to obtain the residual cross-track flow.

Means and standard deviations of the hydrographic Scanfish data that were consecutively recorded within 1 m vertical depth bins at a given position were computed and data lying outside  $\pm 2$  standard deviations from the mean were removed. Means of hydrographic data with 1-m increments were then recalculated and used for interpolation.

Absolute geostrophic velocities along the front were computed for the Scanfish layer and referenced to ADCP velocities at 70 m after tidal velocities were subtracted (Pond and Pickard, 1986). The quality of ADCP current measurements at 70 m was highest because the ringing effect was diminished while the signal to noise ratio remained high. From the absolute geostrophic current estimates that combine hydrography and ADCP current measurements, we were able to study the current structure associated with the Polar Front.

### 2.3. Density ratio and internal Rossby radius of deformation

As a measure of the relative effects of temperature and salinity on the density gradient in the surface front, the dimensionless horizontal density ratio was computed based on Rudnick and Ferrari (1999) as

$$D_x = \frac{\alpha \theta_x}{\beta S_x}, \quad (1)$$

where  $\alpha$  is the thermal expansion coefficient for seawater (describing the change in volume with temperature),  $\beta$  is the haline contraction coefficient (describing the change in volume with salinity), and  $\theta_x$  and  $S_x$  are the horizontal potential temperature and salinity gradients in  $^{\circ}\text{C m}^{-1}$  and  $\text{psu m}^{-1}$ , respectively.

The internal Rossby radius of deformation was computed as

$$R_i = \frac{\sqrt{g'H}}{f}, \quad (2)$$

where  $g' = g \frac{\Delta\rho}{\rho_0}$  is the reduced gravity,  $g$  is the gravity,  $\Delta\rho$  is the density difference between the ArW layer and the underlying AW at the surface expression of the front,  $\rho_0$  is the mean density,  $H$  is the depth of the upper ArW layer, and  $f$  is the Coriolis parameter.

## 3. Results

### 3.1. Hydrography

The strongest sea surface temperature (SST) gradient in the Barents Sea at the time of the survey was in the west along the flank of Spitsbergenbanken indicated by satellite data, where the BSPF is most pronounced (Fig. 1, top). This gradient coincided with the  $6^{\circ}\text{C}$  isotherm. Towards the east, starting near Storbanken, the SST gradient became weaker, corresponding to a broader zone of mixing.

The thermal mixed layer (defined as the depth to the  $27.6\text{ kg m}^{-3}$  isocline) in the study area had a depth of about 25 m and a temperature of about  $6^{\circ}\text{C}$  on the Atlantic side of the Polar Front, and about 15 m and  $5^{\circ}\text{C}$  on the Arctic side (Fig. 2). The internal Rossby radius of deformation (Eq. (2)) was approximately 3 km.

A body of the cold and fresh ArW ( $T < 0^{\circ}\text{C}$ ,  $S < 34.8$ , Loeng, 1991) was present on top of Storbanken on the Arctic side of the front, while the AW ( $T > 3^{\circ}\text{C}$ ,  $S > 35$ , Loeng, 1991) occupied the upper 60 m on the Atlantic side (Fig. 2). Below 60 m, the temperature on the Atlantic side of the front dropped to about  $2^{\circ}\text{C}$ . The coldest ( $T < 2^{\circ}\text{C}$ ) and most saline ( $S \geq 35.1$ ) water on the Atlantic side of the Polar Front was observed along the slope of Storbanken. On the southwestern flank of Storbanken, water with high salinities ( $S > 35$ ) and temperatures between  $2^{\circ}$  and  $3^{\circ}\text{C}$  was submerged beneath a surface layer of relatively fresh and cold water. This led to a surface front separating AW and melt water from the north that was located approximately at the 275 m isobath. The Polar Front between AW and ArW was submerged and coincided with the 125 m isobath along the southwestern flank of Storbanken. The surface front and the Polar Front (in combination referred to as the frontal system below) were about 40 km apart horizontally.

The salinity and temperature gradients across the surface front and the Polar Front were most pronounced over a horizontal distance of about 15 km. The horizontal salinity gradient was strongest in the top 20 m in the surface front, with salinities of 35 on the Atlantic and 34.6 on the Arctic side (Fig. 2, top). This led to a salinity gradient of roughly  $0.03\text{ km}^{-1}$  across the surface front. The horizontal

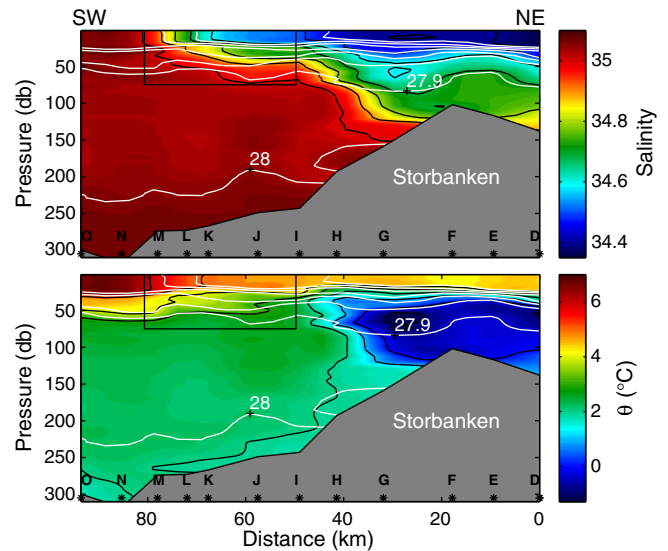


Fig. 2. Hydrography across the Polar Front based on the 12 full-depth CTD stations (marked by black dots along the 300-db isobar, spanning 93 km of section A). Southwest (Atlantic side) is to the left and northeast (Arctic side) to the right. The white contours show isopycnals with an equidistance of  $0.1\text{ kg m}^{-3}$ . Isohalines (top) and isotherms (bottom) with equidistances of 0.1 and  $1^{\circ}\text{C}$ , respectively, are marked in black. The rectangle in the top 75 m shows the extent of the C sections.

temperature gradient in the mixed layer was strongest between the 5° and 6°C isotherms, amounting to a gradient of about 0.07 °C km<sup>-1</sup> (Fig. 2, bottom). Only near the surface, densities on the Atlantic side (~27.5  $\sigma_\theta$ ) were slightly higher than on the Arctic side (~27.3  $\sigma_\theta$ ), establishing a density gradient over 40 km of roughly 0.005 kg m<sup>-3</sup> km<sup>-1</sup> across the surface front. Salinity dominated the density gradient near the surface, since the horizontal density ratio  $D_x$  (Eq. (1)) was approximately 0.6 (<1) with the coefficients  $\alpha$  and  $\beta$  chosen for 5 °C and 34.9 at sea surface pressure.

In the Polar Front, below 75 m, the salinity gradient was only about 0.02 km<sup>-1</sup>, with salinity values of 35 and 34.75 on the Atlantic and Arctic sides, respectively. In contrast to the salinity field, the temperature gradient was largest at the Polar Front. The horizontal temperature gradient was about 0.2 °C km<sup>-1</sup> at 75 m (2.5 °C and -0.5° on the Atlantic and Arctic sides, respectively). Over a distance of only 2 km, the strongest temperature gradient, 0.5 °C km<sup>-1</sup>, was observed at about 25 m between the 2° and 3 °C isotherms. Thermohaline density compensation led to nearly horizontal isopycnals across the subsurface Polar Front.

The pycnocline was strongest on the Arctic side, where it occurred between the 27.3 and 27.8  $\sigma_\theta$  isopycnals over a depth range of about 25 m. On the Atlantic side, it extended over a depth range of about 35 m between the 27.6 and 27.9  $\sigma_\theta$  isopycnals (Fig. 2).  $\theta$ S-profiles across the frontal system spanning a depth range of 75 m covered the greatest density range in the northeast (Arctic side), confirming stronger stratification on the Arctic side compared to the Atlantic side (Fig. 3).

Most of the water on the Atlantic side of the surface front was consistent with the AW definitions by Loeng (1991), while the ArW was exclusively observed in the deepest parts of the northeastern most profiles of section B. PFW (Loeng, 1991) was found in the deepest parts of the central profiles of section B, where the northeastern border of the surface front was located (Fig. 3). In the central  $\theta$ S-profiles of section B and in most profiles of the C sections (not shown), mixing lines were present that nearly followed the isopycnals and connected water mass properties from both sides of the front (Fig. 3). These lines were accompanied by temperature and salinity inversions.

### 3.1.1. Small-scale hydrographic patchiness

A distinct water parcel with lower salinity and temperature than its surroundings was found in the Scanfish layer at a depth of about 30 m on the Atlantic side of the surface front in section A, near the southwestern-most C section (Fig. 4, top, near 20 km). In section B, a saline and relatively warm water parcel surrounded by a relatively

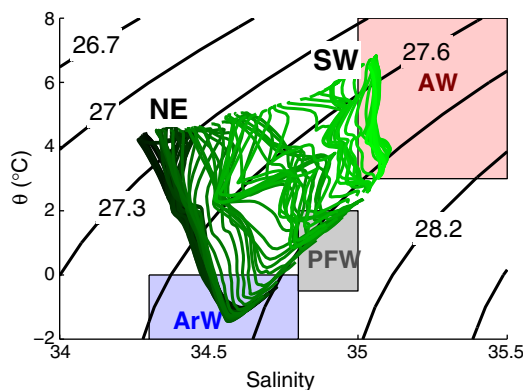


**Fig. 3.**  $\theta$ S-profiles (0 to 75 m) across the frontal system in section B. The southwestern-most profiles (Atlantic side) are shown in light green and labeled with SW. The profiles become increasingly dark towards the Arctic side of the front (labeled NE). Isopycnals with an equidistance of 0.3 kg m<sup>-3</sup> as well as AW, PFW and ArW water masses (Loeng, 1991) are shown in the background.

fresh and cold water mass was observed near the northeastern most C section (Fig. 4, bottom, near 80 km). This warm and saline water parcel was accompanied by doming isopycnals, and had a horizontal diameter of about 10 km.

The hydrographic small-scale variability was particularly conspicuous in the surface front, where the C sections were located (Fig. 5). On the one hand, low density patches on the scale of 5–15 km were found in the mixed layer in the northeastern-most C sections, and a relatively low salinity parcel of water causing low densities was present in the top 20 m in the southwestern most C section. On the other hand, a water mass with higher densities and salinities than the ambient water was observed in the top 20 m in the middle C sections, causing the isopycnals to bend upward there. As in the case of the large-scale cross-frontal density gradients in the surface front, the density anomalies in the distinct water parcels in the C sections were associated with the salinity field, since the salinity and density distributions matched more closely in the top 20 m than the temperature and density fields did (Fig. 5). Between about 40 and 60 m, a layer of comparatively colder and less saline water was observed at the northeastern most C sections. At this depth, both the salinity and the temperature fields matched with the density field.

### 3.2. Circulation

The observed ADCP velocity field was predominantly barotropic, with an exception near the surface and the northeastern-most part of section A. Near the surface, weak baroclinic surface intensified motion was present (Fig. 6, small panels). The dominant flow in the along-front velocity components of sections A and B was a southeastward jet located between the 150 and 250 m isobaths (Fig. 6, big panels). Two cores were present in the jet, the deeper one being located below the surface front, and the lower one being located at the Polar Front closer to Storbanken. The width of the cores was 15–20 km, corresponding to the distance of the most pronounced hydrographic gradients across both fronts. The jet had maximum along-front velocities of 0.20 m s<sup>-1</sup> at its cores in section A. In section B, which was downstream of section A, the velocity components in the deeper core were smaller (~0.10 m s<sup>-1</sup>), while the shallower core's velocity components intensified to about 0.25 m s<sup>-1</sup> from section A to section B. This resulted in an observed velocity difference of approximately 0.15 m s<sup>-1</sup> between the two cores in section B. Along-frontal tidal currents as determined from the AOTIM5 were small (max.  $\pm 0.05$  m s<sup>-1</sup>) compared to the measured along-frontal circulation, and did not influence the dominant along-frontal flow pattern. Tidal influence was only observed on top of Storbanken in the shallowest part of section A. Removal of the tides revealed the baroclinic nature of the currents with a southeastward flow near the bottom and a northwestward flow close to the surface (Fig. 6, top).

A weak northeastward countercurrent with along-front velocity components around 0.05 m s<sup>-1</sup> was measured between the two dominant southeastward cores in section B, as well as south of the frontal jet in sections A and B. Northwestward velocity components of up to 0.10 m s<sup>-1</sup> were observed on top of Storbanken in both sections.

The measured cross-front velocity components in the C sections were weaker than the core velocities in sections A and B (Fig. 7 maximal velocities around  $\pm 0.10$  m s<sup>-1</sup>), with current reversals approximately every 6 h before removal of the tides (not shown). Tidal cross-front velocities were on the same order of magnitude (up to  $\pm 0.095$  m s<sup>-1</sup>) as the observed cross-front ADCP velocities and included current reversals every 6 h. The de-tided cross-front currents were on the order of a few hundredths of m s<sup>-1</sup>, while no regular flow pattern remained (Fig. 7). As in the case of the along-front velocities in sections A and B, the cross-front flow in the C sections was largely barotropic. Vertical structure was only observed on the small scale and near the surface.

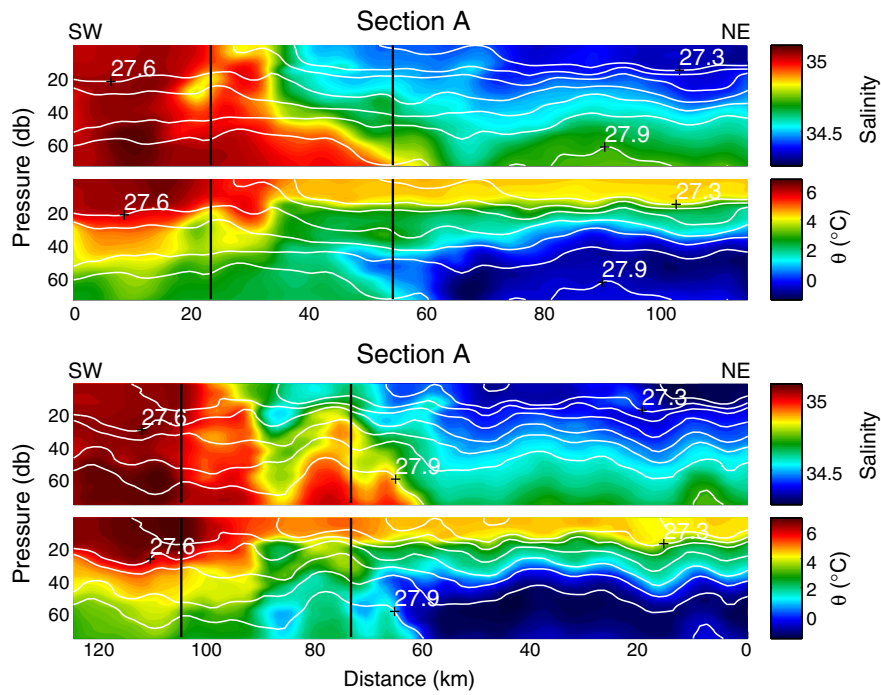


Fig. 4. Hydrography across the surface expression of the Polar Front in sections A and B. Southwest (Atlantic side) and northeast (Arctic side) are to the left and right, respectively. Isopycnals with an equidistance of  $0.1 \text{ kg m}^{-3}$  are shown as white lines. The extent of the C sections is indicated by two vertical black lines.

4. Discussion

4.1. Survey

In this study, high-resolution sampling with a small spatial and temporal coverage was prioritized to resolve the submeso–mesoscale

features of the Barents Sea Polar Front. The short survey time minimized the interpretation problems that can occur when sampling is done from a slow-moving ship in frontal zones with large velocity

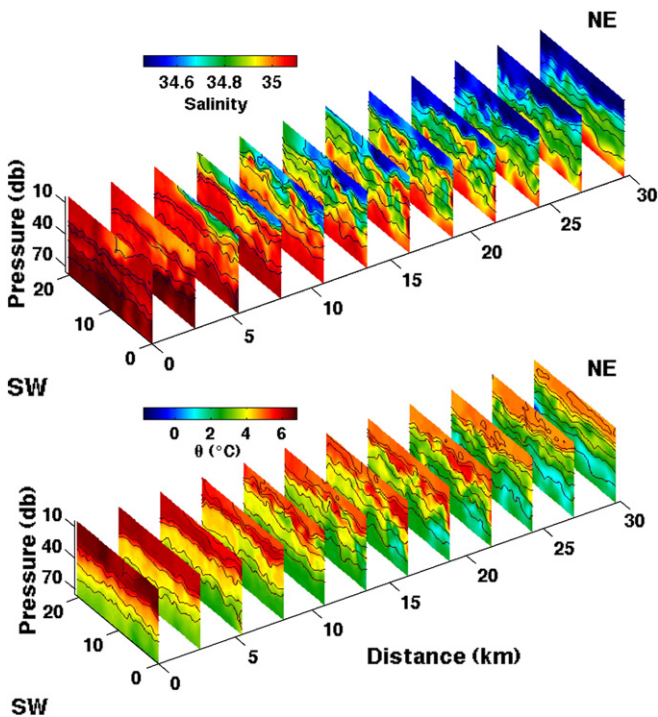


Fig. 5. Hydrography in the surface expression of the Polar Front in the along-front C sections. Southwest (Atlantic side) is to the left and northeast (Arctic side) to the right. Isopycnals with an equidistance of  $0.1 \text{ kg m}^{-3}$  are shown as dark lines.

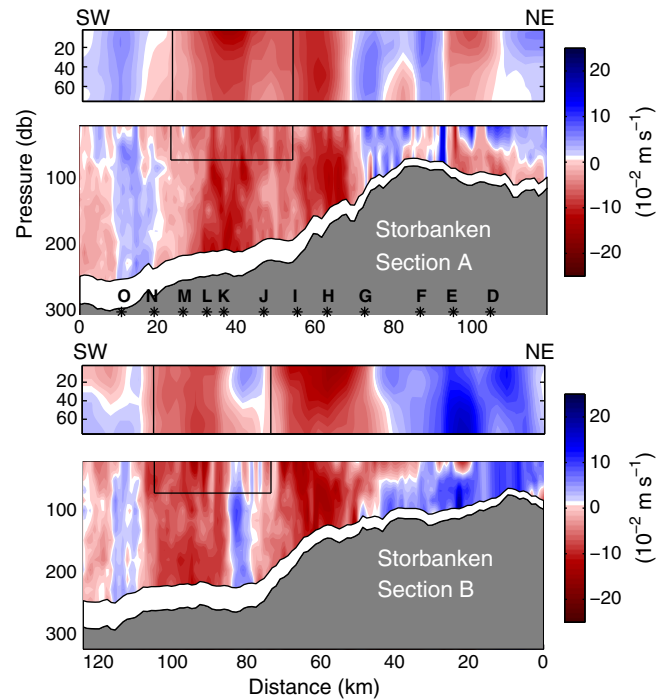
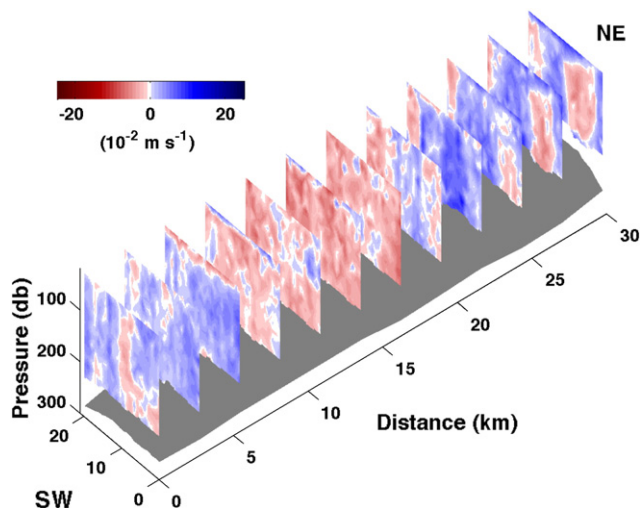


Fig. 6. Absolute along-front geostrophic flow referenced to de-tided ADCP velocities at 70 m (small panels) and the de-tided along-front ADCP velocity (large panels) in section A and B. Positive velocities indicate flow into the page (northwestward), and negative velocities indicate flow out of the page (southeastward). AW is to the left and the ArW to the right in the figure. The 12 CTD stations in section A are marked as in Fig. 2. The black lines in the top 75 m show the extent of the C sections.



**Fig. 7.** De-tided cross-front ADCP velocities from the C sections. Positive velocities are directed northeastward towards the bank and the negative velocities directed south-eastward away from the bank. The Atlantic side (SW) is to the left and the Arctic side (NE) to the right.

shear and advection (Johannessen et al., 1977). Moreover, the small spatial coverage permitted a novel description of submeso–mesoscale variability at the Polar Front that has not been possible before.

The ADCP-derived along-front velocities in sections A and B with a high signal-to-noise ratio and following the topography are assumed to capture the main structure of the frontal circulation. Note, however, that minor current features such as the absence and presence of the weak countercurrent between the two dominant cores in sections A and B, respectively, may be an artifact arising from the undetermined heading bias in the ADCP data.

#### 4.2. Hydrography

The hydrographic mesoscale structure of the summer Polar Front near Storbanken in 2007 was very similar to previous observations of the BSPF. In particular, the horizontal salinity and temperature gradients across the front and the internal Rossby radius of deformation (Eq. (2)) were close to those observed during the Barents Sea Polar Front Experiment (BSPFE) on Spitsbergenbanken. The salinity gradients near the surface were  $0.03 \text{ km}^{-1}$  in the present study and  $0.06 \text{ km}^{-1}$  during the BSPFE, while they were  $0.02 \text{ km}^{-1}$  in both cases below the mixed layer. The temperature gradients near the surface were  $0.07 \text{ }^\circ\text{C km}^{-1}$  in the present study and  $0.11 \text{ }^\circ\text{C km}^{-1}$  during the BSPFE, while they were  $0.20 \text{ }^\circ\text{C km}^{-1}$  in the present study and  $0.22 \text{ }^\circ\text{C km}^{-1}$  in the BSPFE at depth. The internal Rossby radius of deformation was on the order of 3 km in both studies. The  $2^\circ$  and  $3^\circ \text{ }^\circ\text{C}$  isotherms, which best outlined the position of the strongest temperature gradient in the present study ( $0.5 \text{ }^\circ\text{C km}^{-1}$ ), also match findings from the BSPFE and by Johannessen and Foster (1978). At the surface, the strongest temperature gradient occurred between the  $5^\circ$  and  $6^\circ \text{ }^\circ\text{C}$  isotherms, in agreement with satellite data (Fig. 1).

While our data suggest the 34.8 isohaline as a good indicator for both the surface front and the sub-surface BSPF near Storbanken, Parsons et al. (1996) data suggest the slightly less saline 34.6 isohaline at the surface and mid-depth, and the 35 isohaline near the bottom of the front during the BSPFE. The weak density gradient near the surface, which was established by the cross-frontal salinity gradient, is consistent with findings during the BSPFE and in the Arctic Ocean Front (May and Kelley, 2002). Solar heating was most likely responsible for the weak temperature gradient near the surface. The consistencies in the thermohaline structure of the front indicate that the

hydrographic characteristics of the summer BSPF changed little over the last decades.

The cold and saline bottom layer along the flank of Storbanken observed in this study (Fig. 2), may have originated on top of Storbanken in the fall and winter of 2006. On top of Storbanken, salinization processes take place during the fall and winter, forming cold and saline water that flows along the slope of Storbanken throughout the summer (Løyning, 2001).

Local water mass transformation seems to have occurred through surface solar heating of the AW and ArW and through isopycnal mixing. Surface heating is indicated by the  $\theta S$ -profiles, whose upper parts were warmer than conventional definitions for the ArW and PFW in the Barents Sea (Loeng, 1991). Surface heating was probably particularly strong during the present survey, as the SST in summer 2007 was about one standard deviation higher than the long term mean (1971–2000) near Storbanken (Hughes et al., 2008). Isopycnal mixing in the barotropic frontal zone below the mixed layer is manifested in the zig-zag patterns in the  $\theta S$ -profiles (Fig. 3). These mixing processes have been observed in previous summer BSPF studies as well (Parsons et al., 1996).

#### 4.3. Circulation

In contrast to the hydrographic structure, the dominant along-frontal circulation features near the BSPF reported in the literature seem to be less consistent.

The currents in the Barents Sea are primarily barotropic. However, in the area west and south of Storbanken, where the AW sinks below the lighter ArW, the direction of the current in the deep layer has been described to oppose the surface direction (Loeng, 1991). Such counter currents were observed in the ArW flow northeast of the BSPF in section A. Tides had a noticeable effect on the circulation on top of Storbanken, suggesting a tidal mixing regime in the shallow areas of the survey. We also found significant influence of the tidal current on the cross-frontal flow pattern in the surface front, where current reversals approximately every 6 h were likely caused by the M2 tide.

The direction of the dominant along-frontal circulation in this study agrees well with laboratory experiments using a physical model of the Barents Sea that suggest a northeastward warm-core jet of AW on the southeastern slope of Spitsbergenbanken, and a flow towards the 250 m sill between Storbanken and Sentralbanken (Li and McClimans, 1998; McClimans and Nilsen, 1993; Slagstad and McClimans, 2005). Observations by Johansen et al. (1988) also indicate a fluctuating northeastward AW current along the slope of Spitsbergenbanken with currents up to  $0.30 \text{ m s}^{-1}$ . This is in agreement with the major southeastward flow direction and speed of the along-frontal cores observed in this study. On the other hand, a westward flow of AW was observed along the BSPF on the southern flank of Spitsbergenbanken during the BSPFE. This westward flow is thought to have been associated with a barotropic recirculation branch of AW within the Bear Island Trough along the 260 m isobath (Gawarkiewicz and Plueddemann, 1995; Parsons et al., 1996; Skagseth, 2008). (Kowalik and Proshutinsky, 1995) conclude that the generation and maintenance of the BSPF near Bear Island could be explained by tidal mixing and the circulation patterns of AW and ArW. In our study, the topographic confinement near the 260 m isobath of the jet that is associated with the subsurface BSPF matches with predictions of the recirculatory hypothesis of the AW, however, the southeastward direction of the along-frontal flow contradicts this hypothesis. The frontal circulation at Storbanken therefore appears to have been decoupled from the AW recirculation. This is consistent with the findings by Skagseth (Skagseth, 2008), which indicate that the recirculating AW follows a relatively short pathway into the Bear Island Trough before returning to the Norwegian Sea.

Parsons et al. (1996) found a shallow westward geostrophic jet associated with the surface density signature during the BSPFE.

Although our data suggest surface intensified currents associated with the density gradient (small panels Fig. 6), the dominant flow was barotropic and drowned out the baroclinic signal. Satellite altimetry shows that the average sea surface height on Spitsbergenbanken at least in some periods is higher than in most other parts of the Barents Sea (Peacock and Laxon, 2004), suggesting that different large-scale forcing factors may explain the varying frontal dynamics at the southern flank of Spitsbergenbanken and Storbanken.

While our data support the hypothesis that the along-frontal circulation at the BSPF is mainly eastward rather than westward, we conclude that the circulation at the BSPF is too complex and variable to be predicted by simplified models, or to be conclusively described based on individual surveys. Seasonal sea level differences, tidal dynamics, the general flow patterns of the AW and ArW currents, as well as wind may be important for the BSPF flow. Further direct current measurements along the BSPF, ideally over longer periods of time, as well as remote sensing, are necessary to construct a consistent theory of the dynamics driving the frontal circulation in the Polar Front.

#### 4.4. Small-scale variability

The high resolution of the three-dimensional data set revealed a small-scale variability in the hydrographic fields that former studies were not capable of resolving. The hydrographic patchiness in the surface expression of the front was mirrored in the patchy phyto- and zooplankton distributions at the front (Våge, 2010), showing that the variability of the physical fields on the small scale has direct effects on the ecosystem structure near the BSPF.

A small eddy with a diameter of about 15 km may have been present in section B near the surface front, where a parcel of more saline and warmer water was surrounded by a water mass with lower salinity and temperature. This feature was accompanied by doming isopycnals and a narrow countercurrent between the two along-front cores, supporting the eddy hypothesis. However, since the hydrographic data did not extend deep enough to reveal a typical eddy signal, it cannot be concluded that this feature was an eddy.

## 5. Conclusions

The hydrographic structure and characteristics of the summer BSPF, which includes strong temperature and salinity gradients and thermohaline density compensation at depth, appears to be consistent over decades of studies. The circulation at the BSPF, on the other hand, is variable and appears to be driven by different factors over space and time. Cross-frontal flow was influenced by tidal currents, which are likely important for mixing in the frontal system.

The sub-mesoscale variability in the structure of the BSPF was revealed from the present high-resolution data set, which previous surveys could not resolve. These sub-mesoscale features include two cores in the along-frontal jet associated with the surface front and the subsurface Polar Front, as well as hydrographic small-scale patchiness in the surface front on the order of 5 km. These features are all directly relevant for cross-frontal mixing processes and ecosystem dynamics. When planning future field studies in frontal regions and in order to represent mesoscale processes such as fronts and eddies more accurately in future climate models, sub-mesoscale variability should therefore be considered.

## Acknowledgments

Insightful comments from two anonymous reviewers as well as from the JMS guest editor Ken Drinkwater are gratefully acknowledged. Planning and implementation of the field work was conducted as part of

the Norwegian component of the 2007–2008 International Polar Year project Ecosystems Study of Subarctic and Arctic Regions (NESSAR), which was funded by the Norwegian Research Council (project number 176057/S30). We thank the crew of the RV “Jan Mayen” for a successful field experiment.

## References

- Belkin, I.M., Cornillon, P.C., Sherman, K., 2009. Fronts in large marine ecosystems. *Prog. Oceanogr.* 81, 223–236.
- Berezutskii, A.V., Maximov, S.E., Rogionov, V.G., Sklyarov, V.E., 1994. Combined hydrologic and acoustic study of the polar front in the Barents Sea by contact and remote sensing techniques. *Oceanology* 34, 32–36.
- Fanning, A., Weaver, A., 1997. A horizontal resolution and parameter sensitivity study of heat transport in an idealized coupled climate model. *J. Clim.* 10, 2469–2478.
- Furevik, T., 2001. Annual and interannual variability of Atlantic Water temperatures in the Norwegian and Barents Seas: 1980–1996. *Deep Sea Res. Part 1* 48, 383–404.
- Gawarkiewicz, G., Plueddemann, A.J., 1995. Topographic control of thermohaline frontal structure in the Barents Sea Polar Front on the south flank of Spitsbergen Bank. *J. Geophys. Res.* 100, 4509–4524.
- Hansen, C., Samuelsen, A., 2009. Influence of horizontal model grid resolution on the simulated primary production in an embedded primary production model in the Norwegian Sea. *J. Mar. Syst.* 75, 236–244.
- Harris, C.L., Plueddemann, A.J., Gawarkiewicz, G., 1998. Water mass distribution and Polar Front structure in the western Barents Sea. *J. Geophys. Res.* 103, 2905–2917.
- Hughes, S.L., Holliday, N.P., Beszczynska-Möller, A., 2008. ICES Report on Ocean Climate 2007. ICES Coop. Res. Rep. 64 pp.
- Ingvaldsen, R.B., 2005. Width of the North Cape Current and location of the Polar Front in the western Barents Sea. *Geophys. Res. Lett.* 32. doi:10.1029/2005GL023440.
- Ingvaldsen, R., Loeng, H., Asplin, L., 2002. Variability in the Atlantic inflow to the Barents Sea based on a one-year time series from moored current meters. *Cont. Shelf Res.* 22, 505–519.
- Johannessen, O.M., Foster, L.A., 1978. A note on the topographically controlled oceanic Polar Front in the Barents Sea. *J. Geophys. Res.* 83, 4567–4571.
- Johannessen, O.M., Good, D., Smallenburger, C., 1977. Observation of an oceanic front in the Ionian Sea during early winter 1970. *J. Geophys. Res.* 82, 1381–1391.
- Johansen, Ø., Mathisen, J.P., Steinbakke, P., 1988. Environmental data collection in the Barents Sea. OCEANOR Rep. OCN 88059.
- Kowalik, Z., Proshutinsky, A.Y., 1995. Tomographic enhancement of tidal motion in the western Barents Sea. *J. Geophys. Res.* 100, 2613–2637.
- Li, S., McClimans, T.A., 1998. The effects of winds over a barotropic retrograde slope current. *Cont. Shelf Res.* 18, 457–485.
- Loeng, H., 1991. Features of the physical oceanographic conditions of the Barents Sea. *Polar Res.* 10, 5–18.
- Loeng, H., Sundby, S., Østensen, Ø., 1989. Drifting Argos buoys in the Barents Sea. ICES CM Paper C:19, pp. 1–10.
- Løyning, T.B., 2001. Hydrography in the north-western Barents Sea, July–August 1996. *Polar Res.* 20, 1–12.
- May, B.D., Kelley, D.E., 2002. Contrasting the interleaving in two baroclinic ocean fronts. *Dyn. Atmos. Oceans* 36, 23–42.
- McClimans, T.A., Nilsen, J.H., 1993. Laboratory simulation of the ocean currents in the Barents Sea. *Dyn. Atmos. Oceans* 19, 3–25.
- Padman, L., Erofeeva, S., 2004. A barotropic inverse tidal model for the Arctic Ocean. *Geophys. Res. Lett.* 31. doi:10.1029/2003GL019003.
- Parsons, R., Bourke, R.H., Muench, R.D., Chiu, C.S., Lynch, J.F., Miller, J.H., Plueddemann, A.J., Pawlowicz, R., 1996. The Barents Sea Polar Front in summer. *J. Geophys. Res.* 101, 14201–14221.
- Peacock, N.R., Laxon, S.W., 2004. Sea surface height determination in the Arctic Ocean from ERS altimetry. *J. Geophys. Res.* 109. doi:10.1029/2001JC001026.
- Pond, S., Pickard, G., 1986. *Introductory Dynamical Oceanography*, 2 edition. Pergamon Press, Sydney.
- Rixen, M., Allen, J.T., Alderson, S., Cornell, V., Crisp, N., Fielding, S., Mustard, A.T., Pollard, R.T., Popova, E.E., Smeed, D.A., Srokosz, M.A., 2003. Along or across front ocean survey strategy? An operational example at an unstable front. *Geophys. Res. Lett.* 30, 1017.
- Rodionov, V.B., 1992. On the mesoscale structure of the frontal zones in the Nordic seas. *J. Mar. Syst.* 3, 127–139.
- Rudnick, D.L., Ferrari, R., 1999. Compensation of horizontal temperature and salinity gradients on the ocean mixed layer. *Science* 283. doi:10.1126/science.283.5401.526.
- Sakshaug, E., 1997. Biomass and productivity distribution and their variability in the Barents Sea. *ICES J. Mar. Sci.* 54, 341–350.
- Skagseth, Ø., 2008. Recirculation of Atlantic Water in the western Barents Sea. *Geophys. Res. Lett.* 35. doi:10.1029/2008GL033785.
- Slagstad, D., McClimans, T.A., 2005. Modeling the ecosystem dynamics of the Barents Sea including the marginal ice zone: I. Physical and chemical oceanography. *J. Mar. Syst.* 58, 1–18.
- Våge, S., 2010. Structure and dynamics of the Barents Sea Polar Front near the Great Bank and associated plankton distribution in August 2007. Master's thesis. University of Tromsø.